CrystEngComm

PAPER

View Article Online
View Journal | View Issue

Cite this: *CrystEngComm*, 2024, **26**, 4031

Influence of the crystallisation solution environment on the structural pathway from solute solvation to the polymorphic forms of tolfenamic acid†

Yu Liu, [abc] Cai Y. Ma, [b] Junbo Gong [c] and Kevin J. Roberts *[b]

The influence of the solution environment on the solution crystallisation of the conformational polymorphic forms I and II of tolfenamic acid is assessed through integration of multi-scale (molecular, cluster and crystallographic) modelling with polymorphic screening using polythermal crystallisation as a function of solvent selection. Solid-state analysis reveals the contrasting crystal chemistry with the strongest synthon involving hydrogen bonding synthons and π–π van der Waals interactions for forms I and II, respectively. Analysis of the molecular conformational energies reveals molecular structures for forms I and II to be very close which is matched by their calculated lattice energies. Crystallisation as a function of both solute concentration and solution cooling rate reveals form II to be mostly more preferred than form I. The higher stability of the form II conformer together with its easier conformational adjustment during the formation of form II crystals, is consistent with its greater crystallisability compared to the more stable form I. Solute concentration analysis of the relative stabilities of the two forms as a function of their sizes reveals that smaller cluster sizes are required to stabilise the crystal structure for form I with respect to form II. Polymorphic screening as a function of solvent confirms the predicted poor crystallisability of form I whose crystallisation is preferred at higher initial solute concentrations and lower cooling rates in polar solvents but less so for the more apolar solvent toluene, the latter being consistent with π–π solute/solvent interactions promoting the formation of hydrogen bonded solute/solute synthons at the expense of π–π interactions. Modelling work correlates well with the observed crystallisation behaviour, highlighting the importance of understanding solvent selection and solution state structure at the molecular-scale level for directing polymorphic outcomes, as confirmed by the higher crystallisability of the metastable form II.

Received 8th May 2024,
Accepted 8th July 2024

DOI: 10.1039/d4ce00460d

rsc.li/crystengcomm

1. Introduction

Polymorphism is a widely observed phenomenon in the solution crystallisation of organic pharmaceutical compounds and one that can be a significant problem in achieving the precise control of polymorphic form which can, in turn, be crucial in terms of obtaining formulated solid drug products which have the desired physicochemical properties.[1] It is well known that crystallisation process conditions, such as solution supersaturation, processing temperature, solute concentration and solvent type, can influence the assembly of molecular clusters of solute molecules whose structures can template the specific polymorph formed.[2,3] Although significant progress has been made in studying crystallisation kinetics and mechanism, it can still be quite a challenge to fully understand how the kinetic aspects of the crystallisation process can direct the polymorph formation processes. Hence, studies on a diverse range of compounds are needed to characterise the molecular pathway through which the solute in its solvated state within the solution phase is transformed into the formation of solid forms with different polymorphic structures.[2–4]

Characterisation of the structures of the solute entities at their different stages in assembly from nucleation-related clusters to crystals within the crystallisation processes can provide an effective approach to understand the influence of process conditions on polymorphic outcomes. A variety of techniques have been applied to capture both the molecular and super-molecular (synthonic) ordering within these clusters in solution prior to their crystallisation, such as Fourier transform infrared (FTIR) spectroscopy,[5–7] Raman

[a] *School of Chemical Engineering, Shenyang University of Chemical Technology, Shenyang, China*
[b] *Centre for the Digital Design of Drug Products, School of Chemical and Process Engineering, University of Leeds, Woodhouse Lane, Leeds LS2 9JT, UK. E-mail: k.j.roberts@leeds.ac.uk*
[c] *State Key Laboratory of Chemical Engineering, Tianjin University, Tianjin, China*
† Electronic supplementary information (ESI) available. See DOI: https://doi.org/10.1039/d4ce00460d

spectroscopy,[8,9] Ultraviolet–visible (UV/vis) spectroscopy,[10] Nuclear Magnetic Resonance (NMR) spectroscopy[11–15] and X-ray scattering.[5,16–20] Such knowledge can provide structural information on these clusters in terms of their constituent solvent–solute interactions, the size and shape of the solute associates and their molecular conformational distributions. Whilst the crystal structures of the materials at the micro- and macro-scales can be routinely determined using single crystal X-ray diffraction, determination of the structure and development of nano-scale clusters of solute molecules within the solution state can be much more challenging. Nonetheless, through a comparison of the molecular assembly behaviour through the different stages in the overall crystallisation process, the molecular evolution pathway associated with the creation and development of the various polymorphic forms can, in principle, be elucidated.[5,7,21–23]

The development of computational molecular-scale modelling has contributed significantly to the understanding of the thermodynamic properties within the solution state, especially when integrated with experimental data. A variety of molecular-scale computation methods have been successfully applied to the characterisation of the solid state and solution chemistry,[2,5,16,24–41] such as *ab initio* quantum mechanics using density functional theory (DFT) and molecular dynamics (MD) and molecular mechanics (MM) simulations using parametrised empirical interatomic force fields. Although providing high accuracy, DFT calculations and MD simulations can make a significantly high demand on both computer power and calculation time. MM simulations based upon user-defined grid-points have though been found to be effective in identifying the most important molecular–molecular interactions within much shorter simulation times[27] when compared to MD and DFT and hence can provide a suitable platform for the rapid screening of solvents within industrial processes.[35]

Drawing upon the above perspective, in this paper the solution-mediated nucleation pathway associated with the formation of the polymorphic forms of tolfenamic acid (TFA) is examined. TFA (Fig. 1) is a nonsteroidal anti-inflammatory drug with nine reported and closely-related conformational polymorphs.[42–45] Of these, the most encountered polymorphs have been found to be forms I and II and hence these polymorphs form the focus of this study. The main differences between these two forms are reflected in the different molecular conformations within the two crystal structures which is mainly associated with differences in the torsion angle τ (C_7–N_1–C_8–C_{13}) rotation[46] (form I: 75°, form II: 143°), as highlighted in Fig. 1, with the 3D molecular structures of both polymorphic forms being shown in Fig. 4. In this, and under ambient conditions, the stable form I contains the twisted-like molecular conformation, (hereinafter referred to as conformer I), whilst the meta-stable form II contains a more planar-like molecular conformer (hereinafter referred to as conformer II).

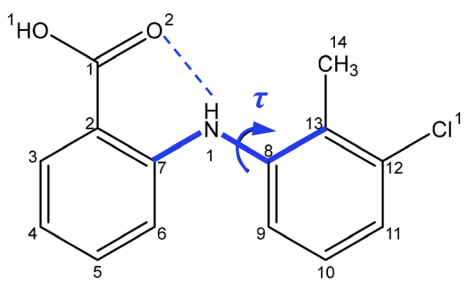

Fig. 1 2D chemical structure of TFA highlighting the important intra-molecular torsion angle τ: C_7–N_1–C_8–C_{13} which is associated with its conformational polymorphic behaviour, and also the intra-molecular hydrogen bond between the amide and carboxylate groups.

With its comparatively simple molecular structure and abundant polymorphic behaviour, TFA has proved to be an attractive model drug compound for studying polymorphism and its control through crystallisation processes, notably for examining the link between the solution state and the resultant crystal structure. Li and coauthors[6,11,47,48] who have made an intensive study of TFA forms I and II and have surprisingly concluded that the stable form I can be crystallised at high supersaturations with the metastable form II being the preferred solid form at low supersaturations.[6] Mindful of this apparent contradiction to Ostwald's rule of stages,[49] solution chemistry studies of TFA using NMR and UV/vis spectroscopy combined with molecular modelling[6,11,47,48] revealed TFA molecules to mainly exist as form II conformer monomers in ethanolic solutions at low concentrations whereas the hydrogen-bonding (HB) dimers of the form I conformers were found to be present at the higher solute concentrations, consistent with the observed crystallisation behaviour at different concentrations. Despite this, Du *et al.*[50] could find no evidence for the formation of HB dimers in ethanol solution either through solution infrared (IR) spectroscopy studies or through related molecular simulations. Repeated fast-cooling crystallisation experiments[50] also seemed to exhibit contrasting results, *i.e.* the metastable crystal form II was found to be more favoured at high supersaturations, which is more consistent with Ostwald's rule.[49] Tang *et al.*[51] further investigated the solution chemistry of TFA using IR spectroscopy and NMR concluding that TFA molecules exist as solvated monomers in ethanol and dimethylformamide, whilst they can form HB dimers in toluene where solute/solvent HB interactions would not be feasible. Whilst these studies concluded that the molecular conformation of TFA in its solution state would appear to be mainly the planar one associated with form II, nonetheless strong solvent–solute interactions were found to increase the proportion of the twisted conformer associated with form I, in particular for ethanol and dimethylformamide. Previous studies on the crystallisability of the polymorphic forms of TFA have been quite limited to date. Liu *et al.*[32] studied the nucleation kinetics of form II as a function of solvent type confirming a progressive nucleation mechanism together with finding strong correlation between solvation strength and nucleation behaviour with the higher solubility hydrogen bonding protic solvents exhibiting lower crystallisability. Related studies on form I crystallisability have not yet

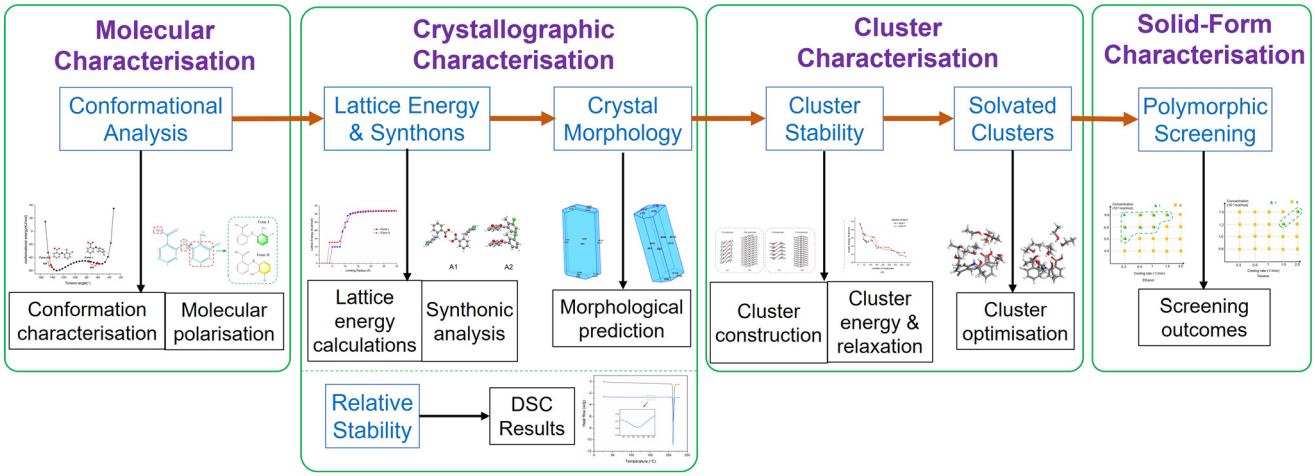

Fig. 2 Structural pathway workflow encompassing molecular-scale modelling and experimental studies of polymorphic screening as a function of solution environment.

appeared in the literature. Detailed studies of the concomitant crystallisation behaviour of TFA[23,52] have further indicated that polymorphic outcomes post-crystallisation can depend on both the solution temperature and solute concentration. Overall, the TFA crystallisation studies to date have concluded that the correlation between nucleation and solution chemistry is strongly influenced by both the strength and directivity associated with the solvation process.

Given that the structural mechanism at the molecular-scale that underpins the linkage between processing conditions and their resultant polymorphic outcomes continue to remain somewhat unclear, further studies are clearly needed. Hence, in this study, the structural pathway from the solvated molecular state through to the crystallisation of either forms I and II has been examined through an integrated (molecule to cluster to crystal) study encompassing both experimental and computational molecular-scale modelling. In this, the molecular conformational and polarisability differences between the molecules present in the form I and form II crystal structures have been examined together with detailed molecular-scale modelling of solute solvation as a function of solvent type. This has been complemented by crystallographic analysis of the TFA crystal chemistry including determination of the energetics of intermolecular interactions in the solid-state. In addition, cluster modelling of solute cluster evolution as a function of their size has been used to examine the relative stability and conformational variability of these two forms at sizes commensurated with the cluster size scales expected in the early stages of the crystallisation process post nucleation. These modelling studies have then been integrated with batch cooling crystallisation experiments carried out under different crystallisation conditions, notably including variations in solvent type, initial solute concentration and solution cooling rate in order to characterise the effects of the solution crystallisation environment on the resultant formation of the two polymorphic forms.

2. Materials and methods

The overall workflow for the work described here is given in Fig. 2 which summarises the methodology and purpose within the structural pathway encompassing molecular-scale modelling and polymorphic screening in different solvents for TFA forms I and II outcomes as a function of crystallisation environment.

2.1 Materials

Tolfenamic acid (>99%), form I, was obtained from Fluorochem Ltd. Form II samples were obtained through recrystallisation with the form obtained being confirmed by powder X-ray diffraction. All solvents (ethanol, methanol, toluene and acetonitrile) were of analytical grade and were purchased from ThermoFisher. All chemicals were used without further purification.

The molecular and crystal structures of TFA form I (ref. code: KAXXAI01 (ref. 42)) and form II (ref. code: KAXXAI[42]) were obtained from the Cambridge Structural Database.[53]

Table 1 Crystallographic data of TFA form I and form II

	Form I[42]	Form II[42]
a (Å)	4.826(2)	3.836(2)
b (Å)	32.128(11)	21.997(5)
c (Å)	8.041(4)	14.205(7)
α (°)	90	90
β (°)	104.88(3)	91.939(4)
γ (°)	90	90
V (A^{-3})	1204.95	1195.54
Space group	$P2_1/c$	$P2_1/n$
Z	4	4
Z'	1	1
Molecular weight (g mol^{-1})	261.70	261.70
Number of HB donors	2	2
Number of HB acceptors	4	4
Number of rotatable bonds	5	5
Density (g cm^{-3})	1.443$^{\text{this study}}$	1.454$^{\text{this study}}$
Void space (%)	26.9$^{\text{this study}}$	24.9$^{\text{this study}}$
Packing coefficient	0.708$^{\text{this study}}$	0.719$^{\text{this study}}$

The crystallographic parameters with some crystal properties of forms I and II are listed in Table 1.

2.2 Experimental methods

2.2.1 Solid-form analysis. The final crystalline forms were characterised by optical assessment, FTIR spectroscopy (Thermo Fisher Scientific iS-10) and differential scanning calorimetry (DSC) (DSC 1 STAR System, Mettler-Toledo, Switzerland).

The standard FTIR spectra for forms I and II are given in Fig. S1 in ESI† evidencing different characteristic peaks for the two forms. All the FTIR spectral data were collected at ambient temperature with a resolution value of 4 cm^{-1}, scan time of 64, and wavenumbers ranging from 400 to 4000 cm^{-1}. Typical spectra of forms I and II exhibited obvious differences in the peak positions (see Fig. S1 (ESI†)) which were used to distinguish between the two polymorphic forms in the analysis of the filtered crystals.

The differences in the colours of the polymorphs were also used as a further aid to confirm the phase transformation time (form II: yellow crystals, form I: white crystals).

Thermal analysis of form I and form II were carried out using DSC to characterise the melting properties and thermal stability of the samples. The measurement was carried out with 5–10 mg samples at a heating rate of 10 °C min^{-1} from 25 to 250 °C under nitrogen purge. The melting point and enthalpy of melting were determined by Mettler Star^e software v10.00.[54]

2.2.2 Crystallisation experiments. TFA solutions were firstly prepared at 50 °C and held for 1 h to give a clear solution, and then transferred to 1.5 ml vials. Four concentrations were chosen for each solvent according to their relative solubilities, *e.g.*, 24, 28, 34, 38 g kg^{-1} for ethanol, 13, 15, 18, 21 g kg^{-1} for methanol, 0.8, 1.0, 1.2, 1.5 g kg^{-1} for toluene and 3, 4, 5.2, 6.2 g kg^{-1} for acetonitrile.

Polythermal crystallisation experiments were carried out using the Technobis Crystal 16[55] platform with the vials individually calibrated with respect to the desired set-point. The crystallisation and dissolution on-sets points during temperature cycling were detected by optical turbidity. The solutions were initially held at 50 °C for 1 hour and then cooled at set cooling rates (0.3, 0.5, 1.0, 1.5, and 2.0 °C min^{-1}) and agitated by constant magnetic stirring at a rate of 700 rpm with each experiment being repeated 16 times. The crystals produced were filtered immediately after formation, and when the optical turbidity decreased within the solution, *i.e.* consistent with the solid-forms being produced in the polythermal experiments being the result of their direct formation by crystallisation and not from any polymorphic phase transformations.

2.2.3 Polymorphic form transformation experiments. 20 mg mixed powder of TFA form I and form II (1 : 1) were added to the 10 ml prepared TFA saturated solutions at given temperatures. Vials of the suspensions were then placed within a temperature controlled shaker which was set to an agitation rate of 400 rpm at temperatures of 5, 20 and 40 °C. The suspensions were examined and analysed every 10 minutes to detect any phase transformation behaviour through filtering a 1 ml suspension for FTIR characterisation. Note that the polymorphic form transformation happened under solution-mediated conditions in slurries.

2.3 Computational molecular modelling

2.3.1 Molecular conformational and polarisability analysis. The potential energy surface of isolated molecules of TFA with respect to the τ_1 torsion angle was generated in the conformer module within the Materials Studio software[56] using the COMPASS II force field with partial electronic charges being calculated using the Gasteiger approach.[57,58] A systematic grid scan method with the torsion angle varying from −180° to 180° in 5° intervals was used based upon a starting molecular geometry built from crystallographic data and optimised using the Forcite module.[56]

The conformational energy of the isolated molecules present within the two polymorphs were calculated in the gas phase by *ab initio* methods using Gaussian09.[59] The single point conformation energies were calculated at the density functional theory level using the 6-311G* basis set and B3LYP dispersion-corrected exchange correlation function. The deformation energetics were calculated through a comparison between the molecular conformation energy present in the crystal structure with that of the optimised free molecule conformation.

2.3.2 Crystal structure analysis. The Python API[53] from the Cambridge Structural Database was used to calculate crystal density, void space (using a probe radius of 0.2 Å and a grid spacing of 0.2 Å)[60] and packing coefficient for both TFA forms I and II. The void space was calculated using the parameters[60] for small pharmaceutical compounds which was found to be consistence with the crystal density and packing coefficient though the parameters used are different *e.g.* from some literature.[61,62]

2.3.3 Intermolecular interactions and lattice energy. The intermolecular pair interaction energies for the dominant intermolecular intrinsic synthons for the two TFA forms were calculated using HABIT98[63,64] using the Dreiding[65] empirical force field together with the partial electronic changes calculated from the semi-empirical quantum mechanics program MOPAC[66] using the Austin Model 1 (AM1) approach. The calculated energies were subdivided into the interaction's constituent van der Waals (vdW), hydrogen bonded and electrostatic energies. The overall crystal lattice energy (E_{latt}) due to inter-molecular packing interactions was summed as a function of radial distance with its convergence being tested by increasing the summation sphere radius up to 30 Å using a step size of 1 Å. The relative inter-atomic contributions within the TFA molecules to the overall lattice energy were obtained by partitioning the lattice energy onto

the different functional groups within the TFA molecule. Through this analysis, the bulk intermolecular interactions (intrinsic synthons) were characterised, classified and ranked in terms of their interaction strengths.

2.3.4 Intermolecular clusters and their energetics as a function of cluster size. The molecular modelling methodology for molecular cluster analysis has been previously described.[30,67,68] In this, the crystal morphology was predicted using the attachment energy (AE) method[69] using HABIT98.[63,64] Face-specific surface attachment energies (E_{att}) were calculated for all the low index crystal planes, as identified using BFDH method.[69–72] These calculations identified those inter-molecular interaction energies (extrinsic synthons) which were terminated by the crystal's external habit faces. These growth promoting attachment energies were taken to be proportional to the relative growth rates of the individual crystal habit faces, hence enabling a 3D simulation of the overall crystal morphology (see *e.g.*[2,69]). Facetted molecular-clusters of different sizes based on the morphological prediction were created by overlaying the predicted morphologies for different cluster sizes with the optimised crystal structure using Mercury program.[73] Size-dependent cluster energies were calculated using Dreiding force-field with Gasteiger[57,58] atomic charges using Materials Studio.[56] The clusters were initially optimised through constraining the molecular conformations with only the inter-molecular packing within the clusters being allowed to vary, hereinafter referred to as minimisation. Following this, the whole structure was relaxed to allow both the molecular positions and conformations to change, hereinafter referred to as relaxation. Through this process, the molecular conformational changes due to the cluster relaxation were analysed by calculating the τ_1 torsion angle distributions as a function of cluster size. In this, the variance parameter (VAR)[30,68] was taken as a measure of conformational adjustment for each the selected cluster size *i.e.* consistent with what could be typical for the early stages of the growth process post-nucleation,[30,68] thus:

$$\mathrm{VAR} = \frac{\sum_{i=1}^{N} \left(T_i - T_{\mathrm{crystal}}\right)}{N-1} \quad (1)$$

where N is the number of molecules in the cluster, T_i represents the torsion-angle value of the ith molecule in the cluster and T_{crystal} represents the torsion-angle within the bulk crystal structure. This analysis was carried out for four representative cluster sizes for the two polymorphic forms, notably 12, 54, 108 and 374 molecules for form I; 11, 50, 114 and 354 molecules for form II, to evaluate the conformational differences at different stages in the cluster evolution. Further explanation of the selection of these cluster sizes is given in Section S7 (ESI†).

2.3.5 Analysis of solute/solute and solute/solvent binding within the solute solvation clusters. Solute/solute and solute/solvent interactions were modelled using intermolecular grid-based search methods[27,29] as described by Rosbottom *et al.*[35] and Kaskiewicz *et al.*[31] This approach examined the energy of interaction between two structural units: a substrate molecular unit (*e.g.* a single molecule in this study) located at the centre of a spatial grid defined around it, and a probe molecule. Intermolecular interactions were calculated as the probe molecule was translated and rotated within the grid. At each molecular position and orientation, the substrate–probe interaction energy was calculated using the empirical atom–atom force field approach of the Dreiding force field[65] with the atomic point charges being calculated using MOPAC AM1 method.[66] In this, the crystallographic conformations for the form I (twisted) and form II (planar) structures[42] were used as substrates with the molecular structures for each solvent (ethanol, methanol, toluene and acetonitrile) as probes. Grid optimisations were performed and an orthogonal grid shape with sizes 25, 30 and 30 Å in the X, Y and Z axis which was found to be suitable for the current study. The number of grid points was set as 10, 15, 15 steps of grid points on the X, Y and Z axis. The Euler rotational steps were set at 30° for the rotation around the x-, y- and z-axis. Overall, the grid search adopted encompassed a search space of 4 866 048 data points encompassing the location and rotation for each simulation.

Subsequently, solvation shell clusters were built by the successive addition of solvent probe molecules whereby the substrate incorporates a probe molecule as located at the highest interaction energy configuration with the molecular pair of substrate and probe molecules becoming the new fixed target for the subsequent probe to find the lowest-energy site, and so on with the process being repeated until an overall solvated solute structural cluster was built up. In this study, a maximum of 10 solvent molecules were used as successive probes with each solute substrate molecule. The resultant clusters were optimised and the cluster energies were calculated using the Forcite module in Material Studio[56] with its Gasteiger atomic point charges.[57,58] In some cases, where the addition of a further probe molecule simply resulted in probe–probe interactions rather than substrate–probe interactions, such interactions were disregarded and the final set of the solvation energies were normalised and ranked with respect to the final substrate/probe coordination number.[32]

Note that, for the widely used HABIT98 (ref. 63 and 64) and SystSearch,[27,29] Dreiding forcefield[65] and MOPAC charge approach[66] were used to calculate the intermolecular pair interaction energies for the two TFA forms. The COMPASS II forcefield with Gasteiger[57,58] partial atomic charges, was utilised for calculations with Materials Studio[56] as MOPAC is not available. Although the different selections may lead to slightly different values calculated, the analysis and conclusions based on these calculated results are expected not to be changed as discussed in literature (*e.g.* ref. 60).

3. Results and discussion

3.1 Molecular properties

3.1.1 Conformational analysis. Analysis of the crystal structures for forms I and II reveal distinctly different molecular conformations due to the rotation of the two single

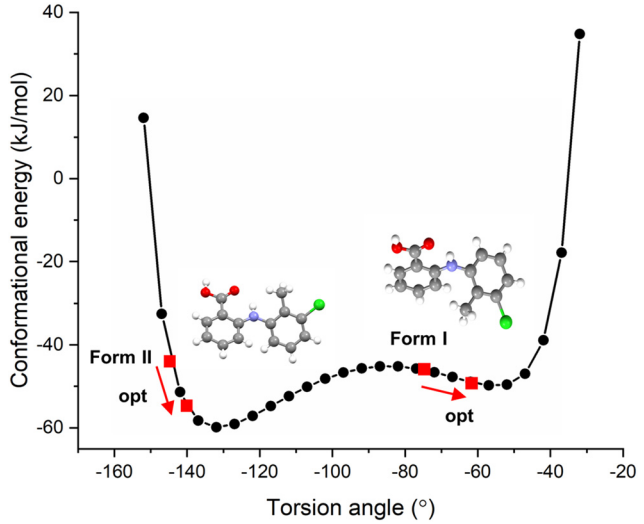

Fig. 3 Calculated molecular conformational energy of TFA as a function of the τ torsion angle with the conformations of the two polymorphs in forms I (twisted conformer) and II (planar conformer) indicated together with their optimisation from crystallographic values.

bonds linking the two benzene rings. As the rotation of the N_1–C_7 bond would be hindered by the N_1–H···O_2 intramolecular interaction between the amide and carboxylate groups, the C_7–N_1–C_8–C_{13} torsion angle (τ, see Fig. 1) was selected to be the most representative measure of the conformational landscape encompassing the differing molecular conformations for the two forms, notably the twisted conformation with a torsion angle of 75° for form I and the planar conformation with a torsion angle of 143° for form II.

The resultant molecular conformational potential energy of TFA as a function of the torsion angle τ is given in Fig. 3, revealing that the conformers present in both the forms I and II structures were located quite close to two local minima positions. The conformer in form II was found to be more stable than that of form I with a lower potential energy which was also found to be much closer to the global minimum conformation energy for an isolated molecule of TFA. However, it is noteworthy that there was not a significantly high energetic barrier between these two conformers consistent with their known concomitant polymorphic behaviour and comparably easy interconversion.[23,32,52] The deformation energies (ΔE_{conf}) for the two forms, given in Table 2, highlight the conformation adjustments that would be expected to be needed to ensure efficient intermolecular close packing within the solid-state. This indicated that the molecule to crystal pathway associated with crystallisation might be expected to be slightly harder for form I when compared to form II. Note that the conformer II with optimised structure was found to be more stable in gas phase based on the calculations using different level of theory though form I indeed exhibits slightly lower conformation energy due to its higher deformation energy when forming a crystal.

3.1.2 Molecular polarisation of the conformers. The calculated electronic charges distribution for the forms I and II conformers revealed several differences in their molecular polarisabilities, as highlighted in dashed red boxes in Fig. 4 (see also atoms highlighted in green in Table S1†). In this, the polar functional groups (mainly –COOH and –NH) were found to be more polarised in form I than in form II, with potential impact on the strength of the intermolecular interactions due to the conformation differences. There were also obvious charge differences on the 3-chloro-2-methylphenyl ring, especially regarding the partial charge difference between the two conformers with the C_{13} atoms having the highest value of 0.0368 highlighting that the rotation angle of this benzene ring might be a key factor in determining the TFA's molecular properties. The change in orientation of the ring between forms I and II reflects a rotation of the ring of form II about the N_1–C_8 bond by 68°, *i.e.* the torsion angle difference between form II (143°) and form I (75°). These changes in the polarisability with the molecular conformation also indicated that molecular conformation change can be expected to affect the crystal chemistry of the two forms, notably in the energetics associated with the formation of π···π aromatic interactions between the benzene rings which would be expected to lead to different strengths for the intermolecular interactions.

3.2 Solid-state properties

3.2.1 Crystallographic intermolecular packing. Comparison between the crystal structures of the two forms in Table 1 reveals that the planar conformer form II is more efficiently packed within the solid state compared to the twisted conformer form I as evidenced by its higher density, lower void space and higher packing coefficient when compared to form I.

3.2.2 DSC analysis. Fig. 5 shows the DSC curves for TFA forms I (white) and II (yellow) revealing that form II transformed to form I over the range of 140–160 °C during heating consistent with an inter-relationship between the two forms, following by the melting point at 211 °C for form I. The former presents a broad transformation peak, consistent with a second order transformation process in contrast to the latter where the form I melting behaviour is characterised by a much sharper first-order peak. This is consistent with the

Table 2 DFT calculation of the single point energy of TFA conformers as associated with the form I and form II extracted directly from crystal structures[42] and the same following optimisation

	Conformation energy, E_{conf} (kcal mol^{-1})	Deformation energy, ΔE_{conf} (kcal mol^{-1})
Conformer in form I crystal structures	−756 565.99	−8.54
Optimised conformer I	−756 557.45	
Conformer in form II crystal structures	−756 564.97	−7.75
Optimised conformer II	−756 557.21	

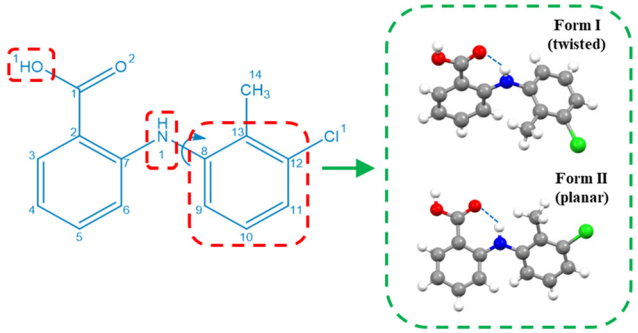

Fig. 4 The molecular structure of TFA displaying the major functional groups in the molecule with the conformation differences between form I and form II (with a torsion angle (C_7–N_1–C_8–C_{13}) difference of 68°) highlighted in dashed green square. The atoms and specific functional groups which showed significant charge differences between form I and form II were highlighted in dashed red squares.

findings in literature,[6,50] indicating that form I is the stable form under ambient conditions. Examination of the melting enthalpies reveals, as might be expected, that the pure form I melting enthalpy (127.73 J g^{-1}) is greater than that of form II (118.97 J g^{-1}) after transformation, indicating a transformation enthalpy of 8.76 J g^{-1} from form II to form I. Interestingly, this is greater than the measured enthalpy of 3.26 J g^{-1} at *ca.* 153 °C which might suggest that this transition might have been taking place gradually over a wider temperature range than that might be immediately evident from the DSC data, perhaps consistent with the quite labile nature of the molecular conformation of TFA and the more closely-packed nature of the form II structure, when compared to form I as revealed from the crystallographic analysis. At this stage, it is not clear whether forms I and II are related monotropically or enantropically and further work is needed to ascertain this.

3.2.3 Solution phase stability analysis. The results of the solution phase stability studies of the forms I and II crystal/

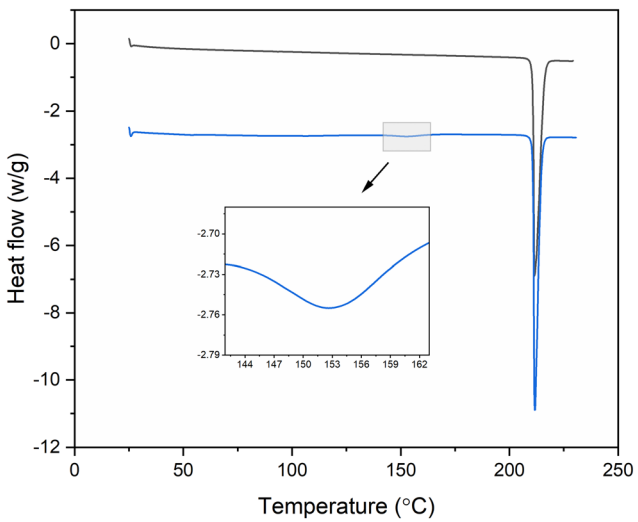

Fig. 5 DSC curves of TFA form I (black) and form II (blue), indicating the transformation of form II to form I.

solution suspensions are given in Table S2 (ESI†), confirming that under ambient conditions form II transforms to form I in all the solvents studied in this research which is in good agreement with the DSC data.

3.2.4 Lattice energies and their convergence behaviour. Fig. 6 gives the lattice energy convergence for forms I and II as a function of the limiting radius which is illustrated through the use of both cumulative and discretised plots. The lattice energy of form II (32.05 kcal mol^{-1}) was found to be slightly larger than the form I (31.8 kcal mol^{-1}), consistent with the dense packing in form II. Nonetheless, the calculations here have only taken into account the intermolecular packing interactions without the contributions from the molecular deformation energy associated with the conformation adjustment needed during the growth process. When the latter is included, the lattice energy of form I (40.34 kcal mol^{-1}) was found to be slightly higher than form II (39.8 kcal mol^{-1}), consistent with the observed stability relationship between the two forms. However, it is noteworthy that these are quite small energetic differences between the two forms consistent with the low energy barrier associated with the transformation between the two conformational polymorphic structures. Overall, this might imply that TFA has quite a labile molecular and intermolecular structure and one enabling, with reasonable ease, conformational change within both the solution- and solid-state environments and hence consistent with concomitant crystallisation behaviour under some experimental conditions.

The first, second and third shells associated with the intermolecular clustering were found to have 2, 25 and 86, and 2, 50 and 51 molecules, respectively, with their energetic contributions to the lattice energy being 31.3%, 63.7% and 5.0%, and 39.8%, 58.3% and 1.9%, for forms I and II, respectively. As shown in Fig. 6(c), form II starts to form its first shell of intermolecular clustering at a smaller size (3 Å) and higher cluster energy than that for the form I clusters. With the increase of cluster size, the form I cluster energies were found to increase rapidly when forming its second shell, gradually exceeding that for form II. The final shell for form I was found to makes a 5% contribution to its overall lattice energy, while form II was only found to contribute 1.9%. Overall, form I was found to converge at a shorter radial distance (12 Å) when compared to form II, consistent with form II generating stable nucleation clusters at smaller first shell sizes than for form I but with the situation reverses for the second shell where form I forms at smaller sizes.

Overall, the data analysis might suggest that variation of solution supersaturation might enable the crystallisation conditions to be manipulated in order to produce smaller cluster sizes, *i.e.* at the higher supersaturations, to control the polymorphic form outcomes. In this, the solubility and crystallisability within a given solvent system could be expected to play an important role as solutions with wider metastable zone widths will potentially generate higher supersaturations. The closeness in these energies, though, is indicative of the challenge regarding single polymorph isolation and hence would be highly consistent with TFA's observed concomitant polymorphic behaviour.

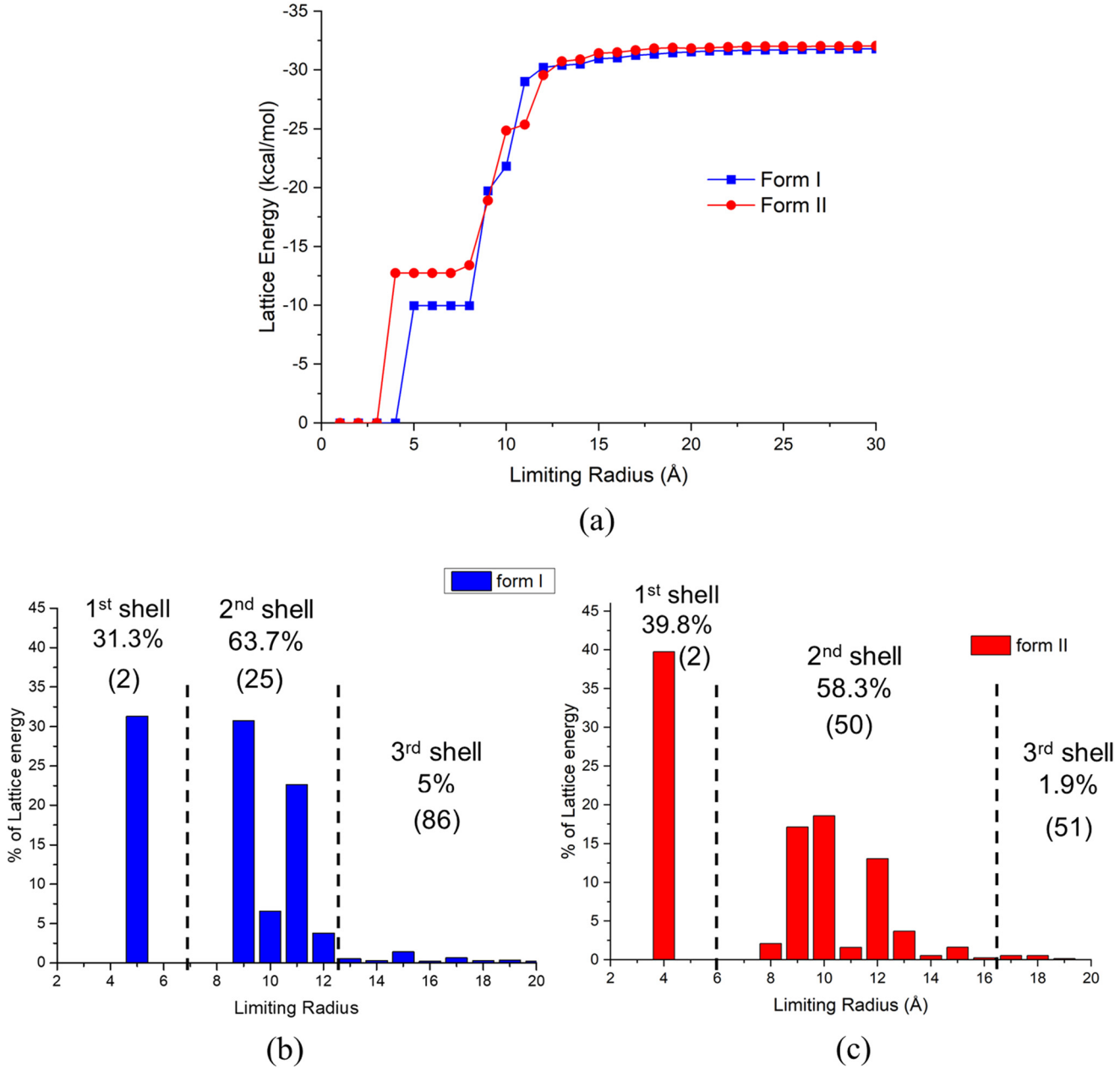

Fig. 6 Convergence behaviour for the total lattice energy: (a) summation convergence data for the two forms; (b) radial discretised distribution plots showing the % contribution to the lattice energy as a function of intermolecular summation distance for form I; and (c) form II. Note that the number of molecules in each shell is showed in bracket.

3.2.5 Analysis of intermolecular interaction types. A breakdown of the relative energetic contributions to the lattice energy for the different types of intermolecular interactions for the two forms is summarised in Table 3. Analysis of the data reveals both forms to have very similar H-bond interactions, albeit those in form II being slightly higher than in form I. A comparison between electrostatic interactions and the vdW components show significant differences in the solid-state chemistry between the two forms with form I showing stronger electrostatic contribution whilst form II has stronger vdW contributions to the lattice energy. The former is consistent with the twisted molecular conformer in the form I structure having a higher polarisability whilst the latter is indicative of the more effective $\pi\cdots\pi$ stacking arrangement between the aromatic rings in the form II structure due to its more planar conformation within the structure.

Examination of the relative contributions of the different molecular functional groups to the lattice energies of the two forms is also provided in Fig. S2 (ESI†). Examination of this reveals no significant differences between the energetic contributions between forms I and II for any of the functional groups in the TFA molecule. Further details can be found in Section S5 (ESI†).

Table 3 Relative contributions of vdW, coulombic energy and H-bond energy to the total lattice energy of TFA form I and form II

Type	Form I	Form II	Percentage contribution to lattice energy %	
			Form I	Form II
vdW (kcal mol^{-1})	−22.51	−24.44	70.79	76.26
Coulombic forces (kcal mol^{-1})	−3.63	−1.76	11.41	5.49
H-bond (kcal mol^{-1})	−5.66	−5.85	17.80	18.25
Lattice energy (kcal mol^{-1})	−31.80	−32.05	100.00	100.00

3.2.6 Intrinsic synthon chemistry of the bulk crystal structures. Fig. 7 presents the intermolecular structures for the dimers associated with the top five strongest synthons within the crystal structures of forms I and II together with in Table 4 more detailed information indicating their respective contributions to the lattice energy. For form I, the strongest synthon (A1) was found to be a hydrogen bond interaction (−4.99 kcal mol^{-1}) with the aromatic stacking dimer (B1) being the second strongest one. The energies of both the A1 and B1 synthons were found to be very similar in terms of their relatively high (about 31% in total) respective contributions to the lattice energy, highlighting that hydrogen bonds and π···π interactions play an important role in stabilising the crystal structure of form I. The other three synthons (C1, D1, E1) were found to be mainly composed of weaker vdW interactions each contributing around 4–6% to the lattice energy. In contrast, the top 5 synthons of form II were found to be distinctly different when compared to those in form I. The strongest synthon (A2) was found to be composed of π···π interactions with a significantly higher energy (−6.73 kcal mol^{-1}) than that of H-bond synthon (B2) (−5.16 kcal mol^{-1}), whilst the other synthons (C2, D2, E2) were found to be mainly weaker vdW interactions each contributing about 2.5–4.5% to the lattice energy.

Comparing the synthons in forms I and II reveal that both the strengths of the shorter range hydrogen bonding synthons and benzene ring stacking interactions in form II are higher than those in form I. However, in contrast the longer range vdW interactions were found to be stronger in form I compared to form II. These differences may reflect form II's planar

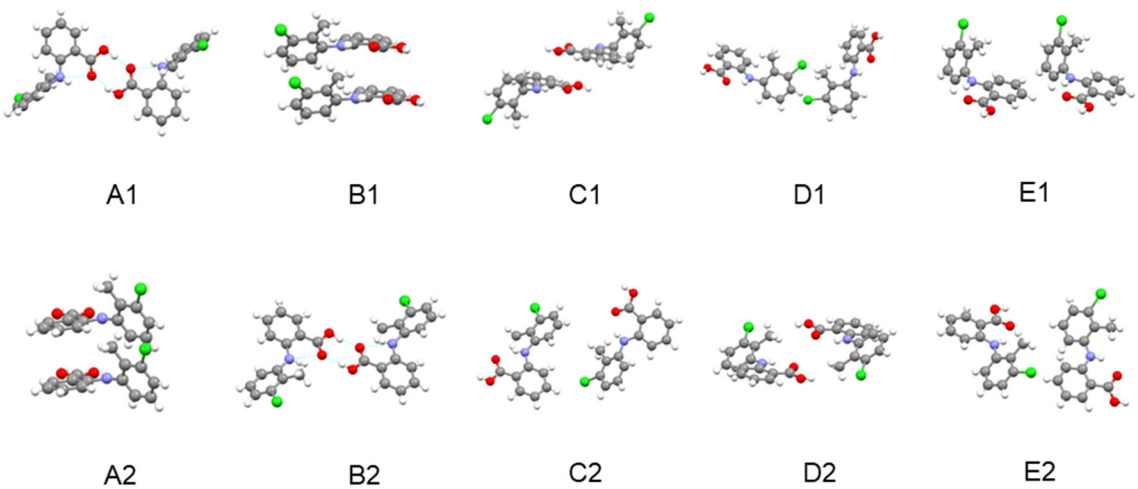

Fig. 7 The intermolecular structural arrangements for dimer pairs of the top five strongest synthons of TFA form I (A1–E1) and form II (A2–E2).

Table 4 Details of the top five synthons in the crystal structure of TFA form I and II along with their contributions to the lattice energy

Form	Synthon	Dispersive energy (kcal mol^{-1})	Columbic energy (kcal mol^{-1})	Total energy (kcal mol^{-1})	Contribution to the lattice energy %	Intermolecular interaction type
I	A1	−2.23	−2.76	−4.99	15.69	H-bond
	B1	−4.93	−0.06	−4.98	15.66	π···π
	C1	−2.34	0.48	−1.86	5.85	vdW
	D1	−1.38	0.01	−1.37	4.31	vdW
	E1	1.06	−0.19	−1.25	3.93	vdW
II	A2	−7.27	0.9	−6.37	19.88	π···π
	B2	−2.26	−2.9	−5.16	16.1	H-bond
	C2	−1.2	−0.23	−1.43	4.46	vdW
	D2	−1.08	0.17	−0.91	2.84	vdW
	E2	−0.92	0.06	−0.86	2.68	vdW

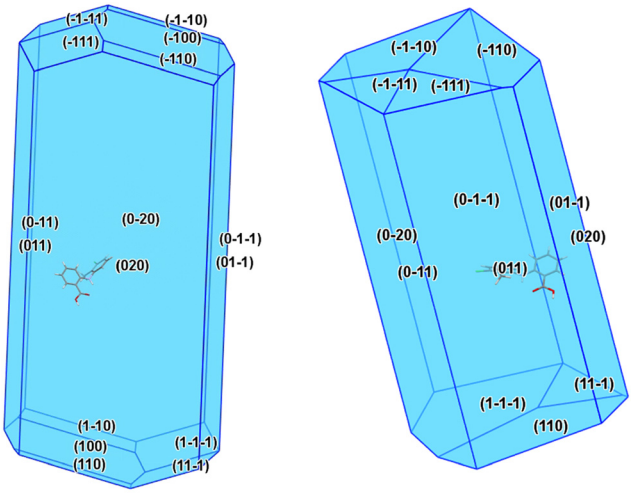

Fig. 8 Predicted attachment energy crystal morphologies for TFA forms I (a) and II (b).

molecular conformation within the crystal structure being more conducive to the efficient stacking of aromatic rings in the initial stages of cluster formation. This would also be consistent with the denser intermolecular packing of this form as well as its tendency to nucleate at higher supersaturations, *i.e.* smaller cluster sizes. In contrast, as the cluster size increases the longer range vdW contributions provide a more favourable environment for the nucleation and growth of the twisted conformers within the stable form I structure and its associated transformation from form II.

3.3 Molecular solute cluster evolution

3.3.1 Predicted crystal morphologies. The attachment energy predicted crystal morphologies for forms I and II are given respectively in Fig. 8(a) and (b) revealing elongated crystal habits for both forms characterised by aspect ratios of *ca.* 2.0 and 2.5, with form I displaying a more tubular crystal habit whilst form II is more needle-like.

3.3.2 Cluster energetic stabilities. The facetted molecular clusters built upon their root crystal structures and their predicted morphologies are shown as a function of their size together with their calculated energies in Fig. 9. The full set of calculations for non-optimised, minimised and relaxed structures are also provided in Fig. S3 (ESI†). Analysis of the data reveals that the stability order as a function of size changes following relaxation of the molecular conformations (Fig. 9(c)) when compared to those for non-optimised and minimised cluster structures. This indicates that the molecular conformational adjustment plays an important role during the early assembly of the crystal structure post-nucleation. With increasing cluster size, two crossover points in terms of the respective cluster energy distributions for forms I and II were found for the optimised clusters at sizes at 20 and 290 molecules, respectively, as shown in Fig. 9(c). When the number of molecules was less than 20, the cluster energies for form II were found to be slightly higher than in form I where the former's more planar conformer permitted strong π–π interactions through synthon A2. When the number of molecules was between 20–290, the clusters of form I were found to exhibit higher energies and higher stability consistent with the build-up of the hydrogen bonding network. However, when the number of molecules was greater than 290, the clusters of form II was again found to be more stable. Similar crossover behaviours were found in the analysis of the cluster energies of L-glutamic acid polymorphic forms.[30,68] The results are also quite consistent with observations in section 3.2.4 from the energy convergence studies that the first shell of form II has a small size but form I converges at a smaller cluster size (180 molecules) compared to form II (340 molecules). For the metastable β- and stable δ-forms of D-mannitol, only a single crossover for the relaxed clusters was found at a cluster size of ~33 molecules,[30] whilst for the stable α- and metastable β-forms of benzophenone, the cluster energies for both forms were found to become very close with the decrease of cluster size.[74] Overall, the closely similar calculated cluster energies for TFA were found to be

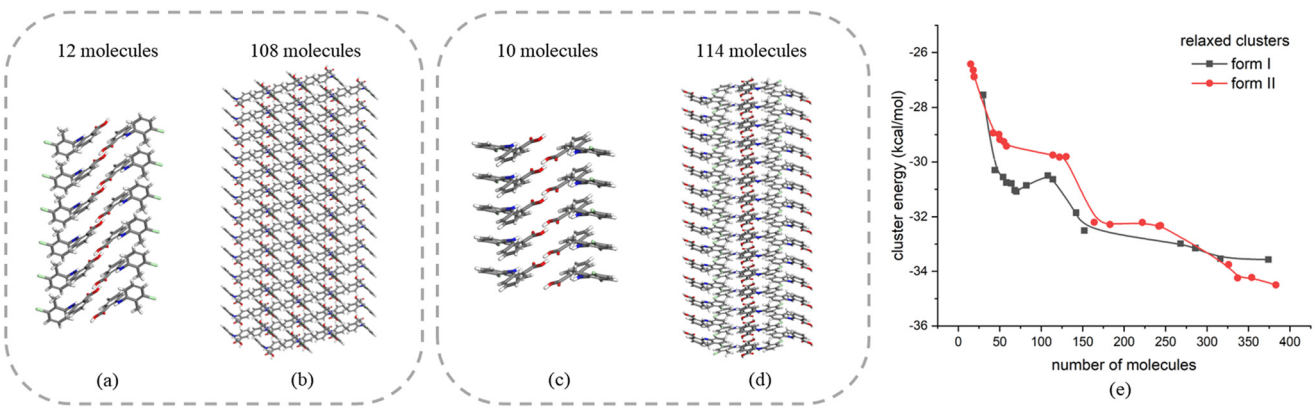

Fig. 9 Facetted molecular clusters of form I (a and b) and form II (c and d) with different sizes; (e) energy of facetted molecular clusters for form I and form II of TFA after structure optimisation.

Table 5 Summary data from the conformational change map for form I and form II

Crystal form	Molecular numbers in a cluster	VAR
Form I	12	15.69
	54	7.81
	108	11.84
	374	8.67
Form II	11	2.01
	50	2.26
	114	1.15
	354	2.85

consistent with this material's observed concomitant polymorphic behaviour.

3.3.3 Conformational analysis of clusters. The results of the conformational analysis for the form I and form II clusters for four representative cluster sizes (Table 5) are shown in Fig. 10. The results reveals that the variation in the torsion angle τ in most of the clusters built from the form I structure were found to be higher than those built from the bulk crystal structures of form II. With increasing cluster size, the distributions of molecular conformation tended to be more constant exhibiting less conformational variability reflecting the fact that a smaller overall fraction of molecule within the clusters would be exposed at the surface where under-coordinated intermolecular interactions might enable their movement. In contrast, analysis of the conformational distributions in form II clusters were found to be consistently

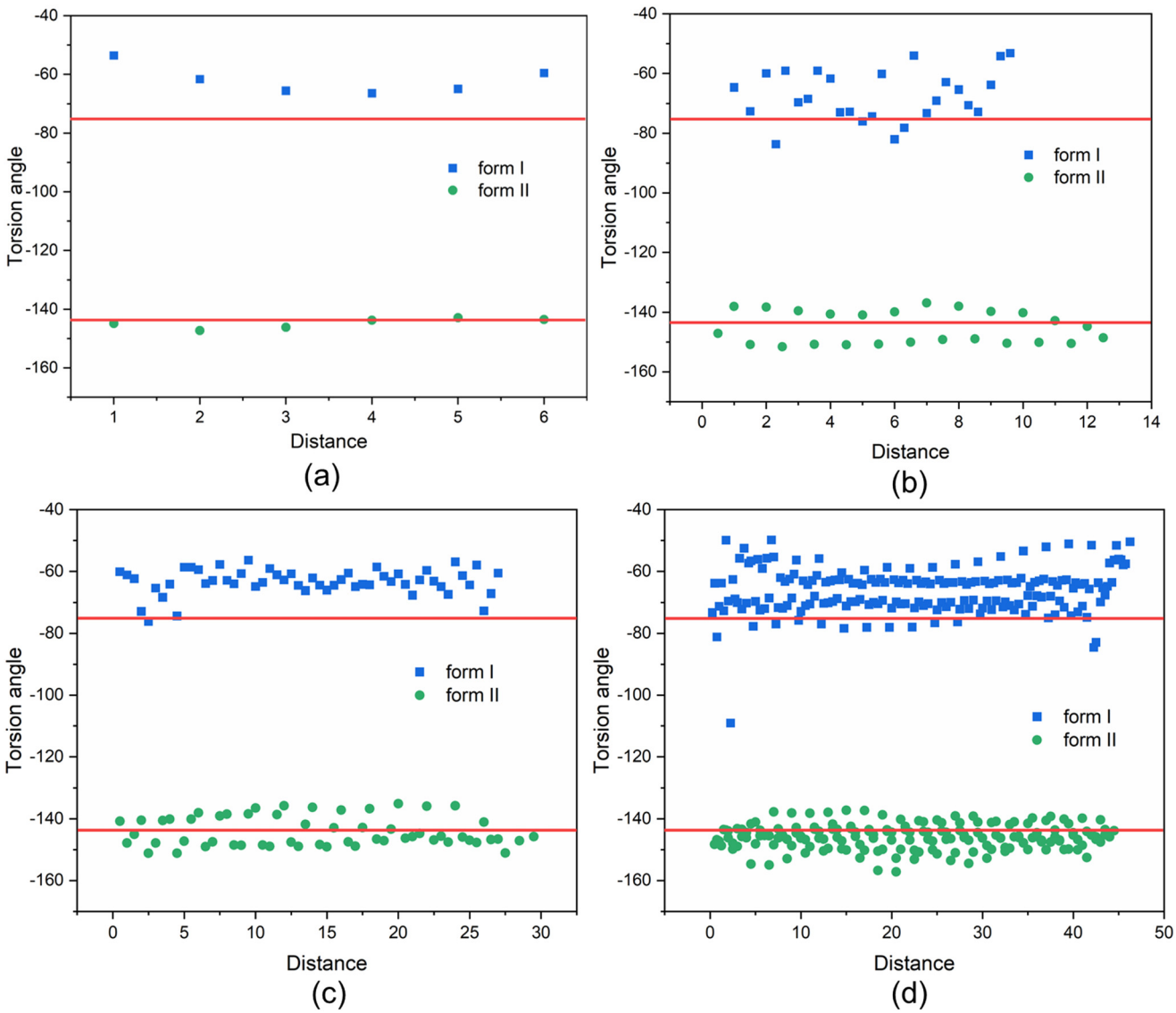

Fig. 10 Torsion angle distribution of molecules in TFA clusters with different sizes for form I and form II. *X*-Axis represents the distance from top face to the other side of the crystal, which is counted by the number of layers. Red lines represent the torsion angles in the crystal structure of form I and form II. (a) Form I: 12 molecules, form II: 11 molecules, (b) form I: 54 molecules, form II: 50 molecules, (c) form I: 108 molecules, form II: 114 molecules, (d) form I: 374 molecules, form II: 354 molecules.

much closer to those observed within the bulk form II crystal structure and were not found to be significantly affected either by their location within the clusters or as a function of the cluster size. Compared to form I, the molecular conformation distributions within the form II clusters clearly exhibited less variability, indicating perhaps an easier conformational adjustment for the pathway from intermolecular assembly to crystallisation for form II when compared to form I.

The above analysis is supported by the calculated VAR values for the clusters of forms I and II at four cluster sizes, given in Table 5. In this, with the increase of cluster size, the torsion angle difference between facetted clusters with those found in the bulk crystal structure were found to gradually decrease for form I whilst no obvious changes were observed for the form II clusters. Overall, for the same cluster size, a larger conformational change was encompassed within the molecular assembly process for form I compared to form II, consistent with higher crystallisability for form II.

3.4 Solute solvation cluster structures and their energies

Fig. 11 shows the results of the construction and minimisation of 10-molecule solvated clusters as a function of solvent selection using either form I or form II conformers as the core central molecule. Examination of the solvated clusters reveals that there were no significant changes in the distributions of solvent molecules between the two conformations as the central molecules. The normalised solvation energies of both forms I (Fig. 11(a–d)) and II (Fig. 11(e–h)) in the four solvents were found to exhibit the same order as characterised by their respective solubilities, *i.e.* ethanol > methanol > toluene > acetonitrile.[32]

In all the solvents, the solvation energy values of the clusters with form II conformer as the central molecule were found to be higher than that with form I, consistent with the solvated structure with form II conformer being more stable when compared to form I conformer. Nonetheless, the energy difference between these two solvated conformers were found to be quite small in most of the solvents, indicating a reasonable probability that both conformers could exist in solution albeit with conformer II being more favoured.

3.5 Polymorph outcomes as a function of crystallisation environment

The polymorphic outcomes resulting from cooling crystallisation experiments in ethanol, methanol, toluene and acetonitrile solutions as a function of different cooling rates and solute concentrations are summarised in Fig. 12 revealing that the polymorphic outcomes were not sharply differentiated under these processing conditions as both forms I and II were often found to concomitantly crystallise under the same conditions, see Fig. S4 (ESI†). The results of the polymorphic screening were found to exhibit a degree of stochastic behaviour at times with both forms I and II crystallising concomitantly under very similar process conditions which highlighted the difficulty in controlling their polymorphic forms *via* crystallisation. In terms of the solution crystallisation conditions, higher initial solute concentrations were found to favour the crystallisation of the stable form I perhaps reflecting a higher probability for solute/solute interactions and hence the molecular assembly of the solute.

The solution cooling rate was also found to affect the crystallisation of form I, with the lower cooling rates

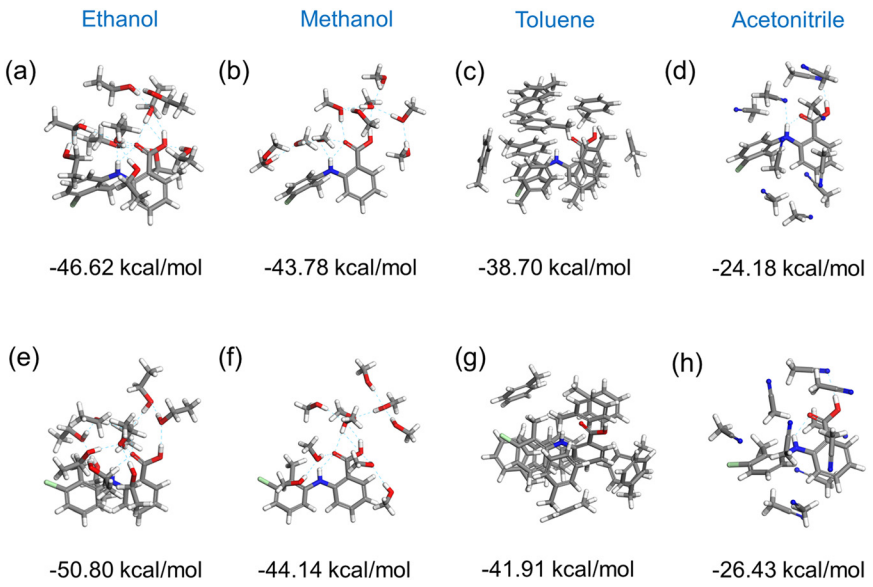

Fig. 11 The optimised 10-molecule solvation clusters with the normalised solvation energies for (a and e) ethanol, (b and f) methanol, (c and g) toluene, and (d and h) acetonitrile, with conformer I (a–d) and conformer II (e–h) of TFA as target respectively.

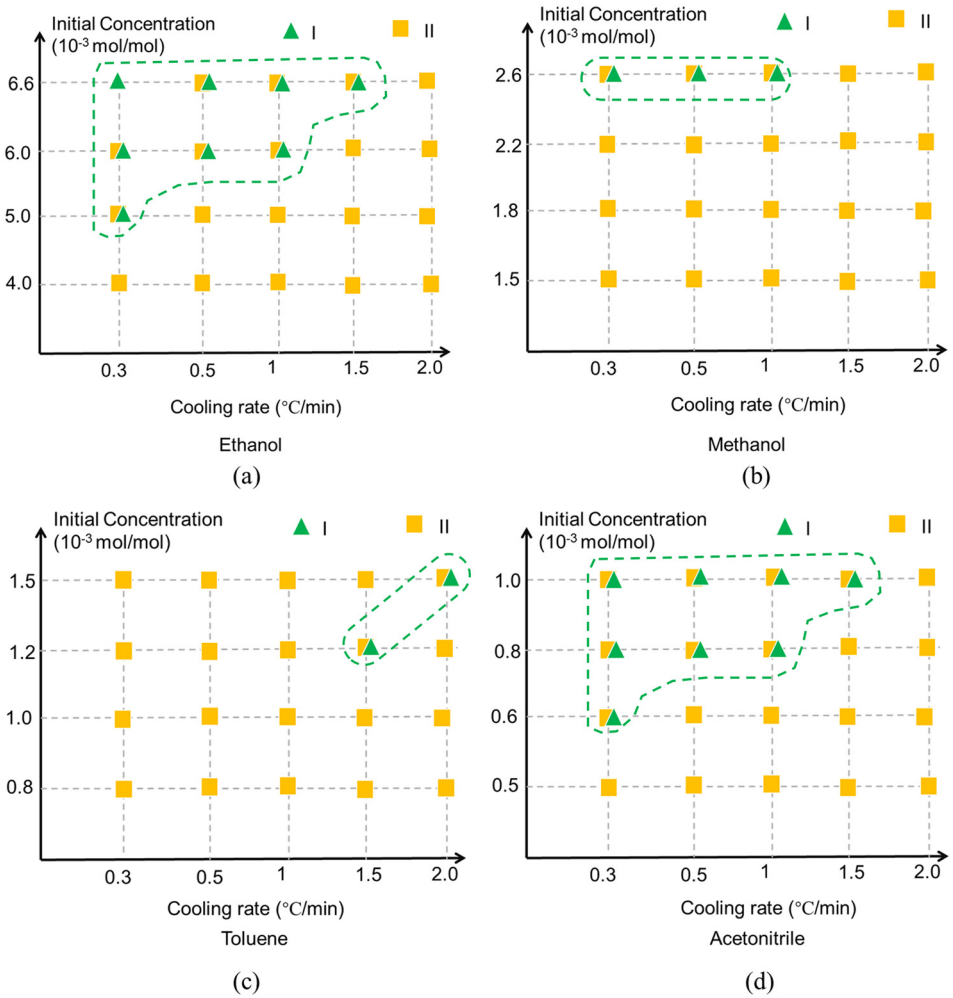

Fig. 12 Crystallisation outcomes of TFA as a function of cooling rate and initial concentration in (a) ethanol, (b) methanol, (c) toluene and (d) acetonitrile. Green triangle represents form I while yellow square represents form II. The overlapping patterns represent that the results are stochastic since form I and form II both have probability to crystallise at the same conditions. The areas highlighted indicate the crystallisation environments favoured by form I.

producing lower supersaturations seemingly increasing the probability of crystallising form I in the polar solvents of ethanol, methanol and acetonitrile albeit with a reverse outcome for the more apolar toluene solutions. Previous studies have shown that solvent selection can have a strong influence on the crystallisability[32] of form II but in this work it appeared to have only a limited impact on the polymorphic outcomes post-crystallisation compared to other process-related factors. The noteworthy exception perhaps was that crystallisation from toluene solutions appeared to show a greater preference for form II crystallisation and less for form I when compared to the other solvents. This contrasting behaviour can perhaps be attributed to the different types of solvent–solute interactions present between the different polar and apolar solvents. The TFA molecule has both hydrogen bonding donor and acceptor sites and thus is able to form strong solute/solvent hydrogen bonds with polar, particularly protic, solvents but obviously this would not be the case in toluene solutions where strong π···π solute/solvent interactions would be expected to dominate.

The contrasting polymorphic behaviour in toluene is supported by the analysis of the synthon energies, notably their order in terms of interaction strength. In this, calculated order was found to be A2 (stacked dimer of conformer II) > B2 (HB dimer of conformer II) > A1 (HB dimer of conformer I) > B1 (stacked dimer of conformer I). Whilst the HB dimer and stacked dimer were found to have contributed equally to the stability of the crystal structure of form I, the stacked dimer was found to be more important in the crystal structure of form II. Hence, it would seem rational that the strong π···π solute/solvent interactions in toluene solutions might influence the assembly of hydrophobic stacked dimers. Thus, the most stable synthon A2 was more likely to be formed in this crystallisation environment while the hydrophilic synthon B2 might be expected to be more difficult to form.

Table 6 Summary of the polymorphic behaviour of TFA forms I and II characterised by multi-scale molecular modelling and crystallisation screening

TFA	Polymorph		Form I	Form II
Molecule	Conformation		Twisted[42]	Planar[42]
	Molecular volume (A^{-3})		1204.95 (ref. 42)	1195.54 (ref. 42)
	Molecular surface area (A^{-2})		233.44	235.65
	Deformation energy (kcal mol^{-1})		−8.54	−7.75
	Dipole moment (D)		1.54	2.77
Cluster	Nucleation mechanism[32]		Unknown	Progressive
	Stability	Smaller sizes	Lower	Higher
		Medium sizes	Higher	Lower
		Larger sizes	Lower	Higher
	Solute cluster conformational variance		7.81–15.69	1.15–2.85
	Solvation energy	Ethanol (protic)	Lower	Higher
		Methanol (protic)		
		Toluene (apolar)		
		Acetonitrile (aprotic)		
Crystal	Lattice energy (kcal mol^{-1})	Dispersive	−22.51	−24.44
		HB	−5.66	−5.85
		Electrostatic	−3.63	−1.76
		Total	−31.80	−32.05
	Strongest two synthons	Energy (kcal mol^{-1})	A1: −4.99 (H-bond) B1: −4.98 (π–π)	A2: −6.37 (π–π) B2: −5.16 (H-bond)
	Close packing		Lower	Higher
	Melting point (°C)		211.0	Converts to form I at (140–160) °C
	Form solution slurry stability		Stable	Converts to form I
Process environment	Influence of solute concentration on polymorphic outcome	Ethanol	Higher solute concentrations	All concentrations
		Methanol	Higher solute concentrations	All concentrations
		Toluene	Higher solute concentrations	All concentrations
		Acetonitrile	Higher solute concentrations	All concentrations
	Influence of cooling rate on polymorphic outcome	Ethanol	Most of cooling rates	All cooling rates
		Methanol	Lower cooling rates	All cooling rates
		Toluene	Higher cooling rates	All cooling rates
		Acetonitrile	Most of cooling rates	All cooling rates
	Overall crystallisability		Lower	Higher

4. Conclusions

Molecular modelling at multiple scales (molecular, intermolecular and crystallographic) combined with crystallisation screening have been used to characterise the influence of the solution processing environment upon the polymorphic crystallisation behaviour of the two main conformational polymorphic forms of TFA. The overall analysis, summarised in Table 6, provides an improvement in the current understanding of the structural pathway for TFA from its solvated solute state through molecular clustering to the formation of crystals. It highlights how the crystallisation process can be affected by the solution environment and how, in turn, the crystallisation processing environment can mediate the formation of the different polymorphic structures.

The studies confirm that, under ambient conditions, the form I structure (twisted conformational state) is more stable than the more close-packed form II structure (planar conformational state). Crystallisation screening studies mostly resulted in the formation of the metastable form II rather than the stable form I, albeit with some variability associated with forms I and II sometimes crystallising concomitantly. The latter reflects the very close similarities in both molecular and solid-state stabilities leading to the polymorphic outcomes being quite challenging to control. The crystallisation of form I requires a greater conformation change in its pathway from its solvated molecular state to the solid-state creating a higher barrier to crystallisation compared to form II. Solute cluster modelling revealed that smaller sizes produced at the higher solution supersaturations are required to stabilise the form II structure compared to form I and that this would be consistent with the former's observed higher crystallisability. Higher solvation energies for all the solvents were found for the form II conformer compared to form I. This indicated the more favourable existence of form II conformer in solutions but with the small energy differences between these two conformational states providing a high probability of co-existence of both conformers, *i.e.* consistent with concomitant polymorphic outcomes. Higher solute concentrations together with slower cooling rates (except for toluene) were also found to promote

the crystallisation of the stable form I, the latter consistent with the Ostwald's rule. Synthon energy analysis reveals the aromatic dimer present in conformer II (synthon A2) to be the strongest intermolecular interaction associated with the formation of form II, whilst HB dimers were found to be more important for the formation of form I rationalising the differential crystallisation behaviour with the polar solvents directing the crystallisation of form II (and also sometimes concomitantly form I) with the apolar solvent toluene being most likely to direct the crystallisation of form II.

The integrated work presented here sheds new light on the generic inter-relationship between the molecular and intermolecular behaviour within the solvated state (coordination, conformation and polarity) through to the formation and relative stability of molecular solute clusters and their concomitant involvement in the crystallisation and polymorph selection behaviour of TFA.

List of symbols and abbreviations

E_{att}	Attachment energy
E_{conf}	Conformation energy
E_{latt}	Lattice energy
N	Number of molecules in a cluster
$T_{crystal}$	Torsion-angle in the bulk crystal structure
T_i	Torsion-angle of the ith molecule in a cluster
X, Y, Z	Cartesian coordinates for grid optimisation
ΔE_{conf}	Deformation energy
τ	Torsion angle
AE	Attachment energy
DFT	Density Functional Theory
DSC	Differential Scanning Calorimetry
FTIR	Fourier Transform Infrared
HB	Hydrogen-bonding
H-bond	Hydrogen-bond
IR	Infrared
MD	Molecular dynamics
MM	Molecular modelling
NMR	Nuclear Magnetic Resonance
ESI	Electronic supplementary information
TFA	Tolfenamic acid
UV/vis	Ultraviolet–visible
VAR	Variance parameter

Data availability

The authors declare that the data supporting the findings of the current study are available within the paper and its ESI.† Should any raw data be needed in another format they are available from the corresponding author upon reasonable request.

Conflicts of interest

The authors declare no competing financial interest.

Acknowledgements

One of us (YL) acknowledges funding support from the China Scholarship Council for a visiting scholarship at the University of Leeds. The authors are grateful for the financial support of Innovate UK through the Digital Design Accelerator Platform Project (TS/T011262/1) in collaboration with AstraZeneca, Cambridge Crystallographic Data Centre, Centre for Process Innovation, GlaxoSmithKline, Perceptive Engineering, Pfizer, Process Systems Enterprises, the University of Sheffield and the University of Strathclyde and also through a Knowledge Transfer Partnership with the Cambridge Crystallographic Data Centre (KTP 12057). This work also builds upon software developments in collaboration with Drs Robert Hammond and Jonathan Pickering at Leeds funded through the ADDoPT and Synthonic Engineering Programs, supported respectively by AMSCI (Grant No. 14060) in collaboration with AstraZeneca, Bristol-Myers Squibb, BRITEST, Cambridge Crystallographic Data Centre, GSK, Perceptive Engineering, Pfizer, Process Systems Enterprise and the STFC Hartree Centre together with the Universities of Cambridge and Strathclyde, and also EPSRC (Grant EP/I028293/1) in collaboration with Pfizer, Boehringer Ingelheim, Novartis, and Syngenta, respectively.

References

1 R. Hilfker, *Polymorphism: in the Pharmaceutical Industry*, John Wiley & Sons, 2006.
2 N. Anuar, S. N. Yusop and K. J. Roberts, *Crystallogr. Rev.*, 2022, **28**, 97–215.
3 R. J. Davey, S. L. M. Schroeder and J. H. ter Horst, *Angew. Chem., Int. Ed.*, 2013, **52**, 2166–2179.
4 L. Derdour and D. Skliar, *Chem. Eng. Sci.*, 2014, **106**, 275–292.
5 I. Rosbottom, T. D. Turner, C. Y. Ma, R. B. Hammond, K. J. Roberts, C. W. Yong and I. T. Todorov, *Faraday Discuss.*, 2022, **235**, 467–489.
6 A. Mattei and T. Li, *Pharm. Res.*, 2012, **29**, 460–470.
7 S. Parveen, R. J. Davey, G. Dent and R. G. Pritchard, *Chem. Commun.*, 2005, 1531–1533, DOI: **10.1039/b418603f**.
8 A. Kwokal, T. T. H. Nguyen and K. J. Roberts, *Cryst. Growth Des.*, 2009, **4**, 4324–4334.
9 S. A. Kulkarni, E. S. McGarrity, H. Meekes and J. H. ter Horst, *Chem. Commun.*, 2012, **48**, 4983–4985.
10 F. Peral and E. Gallego, *Spectrochim. Acta, Part A*, 2003, **59**, 1223–1237.
11 A. Mattei, X. Mei, A.-F. Miller and T. Li, *Cryst. Growth Des.*, 2013, **13**, 3303–3307.
12 I. A. Khodov, S. V. Efimov, M. Y. Nikiforov, V. V. Klochkov and N. Georgi, *J. Pharm. Sci.*, 2014, **103**, 392–394.
13 I. A. Khodov, S. V. Efimov, V. V. Klochkov, G. A. Alper and L. de Carvalho, *Eur. J. Pharm. Sci.*, 2014, **65**, 65–73.
14 W. W. Tang, M. T. Zhang, H. P. Mo, J. B. Gong, J. K. Wang and T. L. Li, *Cryst. Growth Des.*, 2017, **17**, 5049–5053.
15 E. Wiedenbeck, M. Kovermann, D. Gebauer and H. Colfen, *Angew. Chem., Int. Ed.*, 2019, **58**, 19103–19109.

16 D. Toroz, I. Rosbottom, T. D. Turner, D. M. C. Corzo, R. B. Hammond, X. Lai and K. J. Roberts, *Faraday Discuss.*, 2015, **179**, 79–114.
17 D. Pontoni, T. Narayanan and A. R. Rennie, *Langmuir*, 2002, **18**, 56–59.
18 S. Chattopadhyay, D. Erdemir, J. M. B. Evans, J. Ilavsky, H. Amenitsch, C. U. Segre and A. S. Myerson, *Cryst. Growth Des.*, 2005, **5**, 523–527.
19 X. L. Chen, J. Schroder, S. Hauschild, S. Rosenfeldt, M. Dulle and S. Forster, *Langmuir*, 2015, **31**, 11678–11691.
20 J. Polte, R. Erler, A. F. Thunemann, F. Emmerling and R. Kraehnert, *Chem. Commun.*, 2010, **46**, 9209–9211.
21 R. J. Davey, G. Dent, R. K. Mughal and S. Parveen, *Cryst. Growth Des.*, 2006, **6**, 1788–1796.
22 R. A. Chiarella, A. L. Gillon, R. C. Burton, R. J. Davey, G. Sadiq, A. Auffret, M. Cioffi and C. A. Hunter, *Faraday Discuss.*, 2007, **136**, 179–193, discussion 213–129.
23 W. Tang, A. D. Sima, J. Gong, J. Wang and T. Li, *Cryst. Growth Des.*, 2020, **20**, 1779–1788.
24 G. Clydesdale, K. J. Roberts and R. Docherty, *J. Cryst. Growth*, 1994, **135**, 331–340.
25 G. Clydesdale, K. J. Roberts, K. Lewtas and R. Docherty, *J. Cryst. Growth*, 1994, **141**, 443–450.
26 G. Clydesdale, K. J. Roberts, G. B. Telfer and D. J. W. Grant, *J. Pharm. Sci.*, 1997, **86**, 135–141.
27 R. B. Hammond, R. S. Hashim, C. Y. Ma and K. J. Roberts, *J. Pharm. Sci.*, 2006, **95**, 2361–2372.
28 R. B. Hammond, S. Jeck, C. Y. Ma, K. Pencheva, K. J. Roberts and T. Auffret, *J. Pharm. Sci.*, 2009, **98**, 4589–4602.
29 R. B. Hammond, C. Y. Ma, K. J. Roberts, P. Y. Ghi and R. K. Harris, *J. Phys. Chem. B*, 2003, **107**, 11820–11826.
30 R. B. Hammond, K. Pencheva and K. J. Roberts, *CrystEngComm*, 2012, **14**, 1069–1082.
31 P. L. Kaskiewicz, I. Rosbottom, D. M. Camacho Corzo, R. B. Hammond, R. Downie, P. J. Dowding, N. George and K. J. Roberts, *CrystEngComm*, 2021, **23**, 3109–3125.
32 Y. Liu, C. Y. Ma, J. Gong and K. J. Roberts, *Cryst. Growth Des.*, 2023, **23**, 5846–5859.
33 C. Y. Ma, A. Kwokal, D. Getches, Y.-W. Hsiao and K. J. Roberts, *Cryst. Growth Des.*, 2023, **23**, 4522–4537.
34 K. J. Roberts, R. B. Hammond, V. Ramachandran and R. Docherty, in *Computational Approaches in Pharmaceutical Solid State Chemistry*, ed. Y. A. Abramov, John Wiley & Sons, Ltd, 2015, pp. 175–210.
35 I. Rosbottom, J. H. Pickering, R. B. Hammond and K. J. Roberts, *Org. Process Res. Dev.*, 2020, **24**, 500–507.
36 I. Rosbottom, K. J. Roberts and R. Docherty, *CrystEngComm*, 2015, **17**, 5768–5788.
37 I. Rosbottom, C. W. Yong, D. L. Geatches, R. B. Hammond, I. T. Todorov and K. J. Roberts, *Mol. Simul.*, 2021, **47**, 257–272.
38 T. D. Turner, N. Dawson, M. Edwards, J. H. Pickering, R. B. Hammond, R. Docherty and K. J. Roberts, *Cryst. Growth Des.*, 2022, **22**, 3042–3059.
39 C. Wang, I. Rosbottom, T. D. Turner, S. Laing, A. G. P. Maloney, A. Y. Sheikh, R. Docherty, Q. Yin and K. J. Roberts, *Pharm. Res.*, 2021, **38**, 971–990.
40 C. Wang, T. D. Turner, C. Y. Ma, C. M. Pask, I. Rosbottom, R. S. Hong, A. Y. Sheikh, Q. Yin and K. J. Roberts, *CrystEngComm*, 2023, **25**, 1782–1791.
41 C. Wang, C. Y. Ma, R. S. Hong, T. D. Turner, I. Rosbottom, A. Y. Sheikh, Q. Yin and K. J. Roberts, *Mol. Pharmaceutics*, 2024, **21**, 3525–3539.
42 K. V. Andersen, S. Larsen, B. Alhede, N. Gelting and O. Buchardt, *J. Chem. Soc., Perkin Trans. 2*, 1989, **2**, 1443–1447.
43 P. Sacchi, S. M. Reutzel-Edens and A. J. Cruz-Cabeza, *CrystEngComm*, 2021, **23**, 3636–3647.
44 V. Lopez-Mejias, J. W. Kampf and A. J. Matzger, *J. Am. Chem. Soc.*, 2009, **131**, 4554–4555.
45 D. H. Case, V. K. Srirambhatla, R. Guo, R. E. Watson, L. S. Price, H. Polyzois, J. K. Cockcroft, A. J. Florence, D. A. Tocher and S. L. Price, *Cryst. Growth Des.*, 2018, **18**, 5322–5331.
46 A. O. Surov, P. Szterner, W. Zielenkiewicz and G. L. Perlovich, *J. Pharm. Biomed. Anal.*, 2009, **50**, 831–840.
47 A. Mattei and T. Li, *Int. J. Pharm.*, 2011, **418**, 179–186.
48 A. Mattei and T. Li, *Cryst. Growth Des.*, 2014, **14**, 2709–2713.
49 W. Ostwald, *Phys. Chem.*, 1897, **22**, 289–330.
50 W. Du, A. J. Cruz-Cabeza, S. Woutersen, R. J. Davey and Q. Yin, *Chem. Sci.*, 2015, **6**, 3515–3524.
51 W. Tang, H. Mo, M. Zhang, S. Parkin, J. Gong, J. Wang and T. Li, *J. Phys. Chem. B*, 2017, **121**, 10118–10124.
52 W. W. Tang, Y. F. Quan, J. B. Gong, J. K. Wang, Q. X. Yin and T. L. Li, *AIChE J.*, 2021, **67**, e17129.
53 C. R. Groom, I. J. Bruno, M. P. Lightfoot and S. C. Ward, *Acta Crystallogr., Sect. B: Struct. Sci., Cryst. Eng. Mater.*, 2016, **72**, 171–179.
54 Mettler-Toledo, DSC 1 STAR System, Mettler-Toledo, Switzerland (**https://www.mt.com/**).
55 Technobis Crystallization Systems, Technobis Crystallization Systems B.V. (**https://www.crystallizationsystems.com/products/crystal16/**), Pyrietstraat 2, 1812 SC Alkmaar, The Netherlands).
56 Dassault Systèmes, *BIOVIA Materials Studio 2019*, (**https://www.3ds.com/products-services/biovia/products/molecular-modeling-simulation/biovia-materials-studio/**), 78946 Vélizy-Villacoublay Cedex, France.
57 J. Gasteiger and M. Marsili, *Tetrahedron Lett.*, 1978, 3181–3184.
58 J. Gasteiger and M. Marsili, *Tetrahedron*, 1980, **36**, 3219–3228.
59 M. J. Frisch, G. W. Trucks, H. B. Schlegel, G. E. Scuseria, M. A. Robb, J. R. Cheeseman, G. Scalmani, V. Barone, G. A. Petersson, H. Nakatsuji, X. Li, M. Caricato, A. Marenich, J. Bloino, B. G. Janesko, R. Gomperts, B. Mennucci, H. P. Hratchian, J. V. Ortiz, A. F. Izmaylov, J. L. Sonnenberg, D. Williams-Young, F. Ding, F. Lipparini, F. Egidi, J. Goings, B. Peng, A. Petrone, T. Henderson, D. Ranasinghe, V. G. Zakrzewski, J. Gao, N. Rega, G. Zheng, W. Liang, M. Hada, M. Ehara, K. Toyota, R. Fukuda, J. Hasegawa, M. Ishida, T. Nakajima, Y. Honda, Y. Kitao, H. Nakai, T. Vreven, K. Throssell, J. A. Montgomery Jr, J. E. Peralta, F. Ogliaro, M.

Bearpark, J. J. Heyd, E. Brothers, K. N. Kudin, V. N. Staroverov, T. Keith, R. Kobayashi, J. Normand, K. Raghavachari, A. Rendell, J. C. Burant, S. S. Iyengar, J. Tomasi, M. Cossi, J. M. Millam, M. Klene, C. Adamo, R. Cammi, J. W. Ochterski, R. L. Martin, K. Morokuma, Ö. Farkas, J. B. Foresman and D. J. Fox, *Gaussian~ 09 Revision D. 02*, 2016.

60 C. Y. Ma, A. A. Moldovan, A. G. P. Maloney and K. J. Roberts, *J. Pharm. Sci.*, 2023, **112**, 435–445.

61 L. J. Barbour, *Chem. Commun.*, 2006, 1163–1168.

62 C. F. Macrae, I. Sovago, S. J. Cottrell, P. T. A. Galek, P. McCabe, E. Pidcock, M. Platings, G. P. Shields, J. S. Stevens, M. Towler and P. A. Wood, *J. Appl. Crystallogr.*, 2020, **53**, 226–235.

63 G. Clydesdale, R. Docherty and K. Roberts, *J. Cryst. Growth*, 1996, **166**, 78–83.

64 G. Clydesdale, R. Docherty and K. J. Roberts, *Comput. Phys. Commun.*, 1991, **64**, 311–328.

65 S. L. Mayo, B. D. Olafson and W. A. Goddard, *J. Phys. Chem.*, 1990, **94**, 8897–8909.

66 J. J. P. Stewart, *Quant. Chem. Prog. Exchange*, 1985, **5**, 62–63.

67 R. B. Hammond, K. Pencheva, V. Ramachandran and K. J. Roberts, *Cryst. Growth Des.*, 2007, **7**, 1571–1574.

68 R. B. Hammond, K. Pencheva and K. J. Roberts, *J. Phys. Chem. B*, 2005, **109**, 19550–19552.

69 R. Docherty, G. Clydesdale, K. J. Roberts and P. Bennema, *J. Phys. D: Appl. Phys.*, 1991, **24**, 89–99.

70 A. Bravais, *Etudes Cristallographiques*, Gauthiers-Villars, Paris, 1866.

71 G. Friedel, *Bull. Soc. Fr. Mineral. Cristallogr.*, 1907, **30**, 326–455.

72 J. D. H. Donnay and D. Harker, *Am. Mineral.*, 1937, **22**, 446–467.

73 C. F. Macrae, I. J. Bruno, J. A. Chisholm, P. R. Edgington, P. McCabe, E. Pidcock, L. Rodriguez-Monge, R. Taylor, J. Van De Streek and P. A. Wood, *J. Appl. Crystallogr.*, 2008, **41**, 466–470.

74 R. B. Hammond, K. Pencheva and K. J. Roberts, *Faraday Discuss.*, 2007, **136**, 91–106.